ELSEVIER

Sequential thermal modelling of the spray-forming process

Dirk Bergmann, Udo Fritsching *

Research Centre "Spray Forming" SFB 372, University of Bremen, Badgasteiner Str. 3, 28359 Bremen, Germany

Abstract

Three modules describing metal behaviour during sequential stages of the spray-forming process are coupled in this contribution to provide an integrated thermal simulation of the process. These sub-models describe the melt delivery to the atomizer (tundish), the spray, and the consolidation. Process properties of particular concern in these models are the melt cooling rates and residence times in the various stages of the spray-forming process, and the interface conditions between the spray and the deposit, where the sprayed material impinges onto the substrate or surface of the deposit. The input parameters for each successive sub-model are delivered by the preceding module.

The tundish module describes the heat and melt flow behaviour in the tundish, and the spray simulation module defines the multi-phase flow in the spray by considering properties of individual particles. The thermal energy inputs for the deposit module are derived from the spray model by specific averaging procedures. The solidification and cooling parameters of the deposit are then derived in the consolidation module.

These sequential modules describe the thermal behaviour of a melt element throughout all the successive stages in the spray-forming process, from atomization in the liquid state via the spray stage and compaction to the final cooling (to room temperature).

Using the coupled model, main process parameters are varied and their influence is discussed.
© 2003 Elsevier SAS. All rights reserved.

Keywords: Spray forming; Integrated thermal model; Tundish flow; Metal spray; Consolidation

1. Introduction

Spray-forming is a metallurgical process that enables production of near-net shaped metallic preforms that have very interesting properties [1–3]. In this process, the melted and superheated metal is atomized, usually by inert gases in the first stage. In the spray, the molten metal droplets are cooled and partially solidify as heat is lost to the cold spray gas. The smaller particles immediately solidify, while the largest particles remain fully liquid until they reach a size-dependent distance from the atomizer. The medium sized particles are typically in a state of phase change (solidification). The spray particles impinge onto the surface of a substrate or already compacted deposit. In the upper part of the deposit, a semi-solid area called the "mushy zone" or "mixing layer" is formed by consolidation of the spray. In this way, the deposit steadily grows, in a manner governed by the properties of the spray and the shape and movement of the substrate. Typical forms of deposits

produced by spray formation include billets, sheets and strips, and tubes. Materials used in this process include steel, copper or aluminium alloys, superalloys, and metal-matrix-composites (MMC).

In order to maximize the scope of spray-forming, it is essential to describe the physical transition in the mushy layer in the upper parts of the deposited material as accurately as possible. Depending on operational conditions, the geometric extent and residence time of the mushy zone may vary strongly. Therefore, the functions presented here have been developed to describe the thermal behaviour of a melt element from the melt delivery in the tundish, via the spray phase to the consolidation of the deposit. This thermal behaviour essentially determines the properties of the resulting spray-formed product.

The value of numerical modelling and simulation for investigating the complex interaction of parameters and conditions in the spray-forming process has been widely acknowledged. Analysis of this process typically involves subdivision of the entire process into sub-processes, which are then modelled individually by appropriate approaches. Most interest within the spray-forming process has been fo-

---

* Corresponding author.
  E-mail address: ufri@iwt.uni-bremen.de (U. Fritsching).

Nomenclature

c_{pl}	specific heat capacity of the liquid material	$J\cdot kg^{-1}\cdot K^{-1}$
c_{ps}	specific heat capacity of the solid material	$J\cdot kg^{-1}\cdot K^{-1}$
d_{exit}	tundish exit diameter	m
d_p	particle diameter	m
D	deposition function	
f_s	solid fraction	
$f_{s,h}$	mean solid fraction (enthalpy method)	
$f_{s,m}$	mean solid fraction (separation method)	
GMR	gas to melt mass flow ratio	
h	liquid melt height in the tundish	m
$\overline{h_p}$	averaged specific enthalpy of the particle mass	$J\cdot kg^{-1}$
Δh_f	specific solidification enthalpy (latent heat)	$J\cdot kg^{-1}$
m_p	particle mass	kg
Nu	Nusselt number	
Pr	Prandtl number	
q_0	number density distribution	$1/\mu m$
r	radius	m
Re	Reynolds number	
s	flight distance of droplets/particles	m
t	time	s
T	temperature	K
T_h	mean temperature (enthalpy method)	K
T_l	liquidus temperature	K
T_m	mean temperature (separation method)......	K
T_p	particle temperature	K
T_s	solidus temperature	K
ΔT_l	melt superheat (temperature above liquidus).	K
Tu	turbulence intensity	
x	normal distance from the substrate surface ..	m
x_{max}	maximum deposit height	m
z	distance from atomizer to substrate	m

cussed on the spray behaviour. Here, several models with differing degrees of complexity have been proposed [4–8], while formation of the pre-form and the transient thermal behaviour have been studied in [9–12]. In addition, important material properties, such as the possible formation of pores and the grain size distribution, have been modelled from the thermal conditions of the pre-form during the process [13–16]. Approaches for coupling some individual models of the spray-forming process can also be found, e.g., in [3,7,17,18].

In the present contribution, thermal modelling modules are coupled to describe the thermal behaviour of a melt element during successive stages of the spray-forming process, as illustrated in Fig. 1, from melt delivery in the tundish and atomization in the liquid state via the spray formation and to the compaction stage. The input parameters for each sub-model are derived from the results of the preceding module.
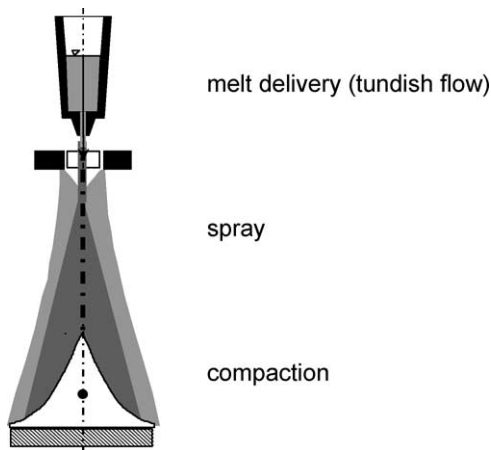

Fig. 1. Stages of integrated sequential spray forming model.

Using the coupled model, main process parameters are varied and their influence on the thermal history is discussed.

2. Tundish flow model

In a typical spray-forming process, the melt is poured from the crucible into a tundish where a constant melt height is maintained in order to control the metal's flow rate. Modelling of the melt flow and cooling in the tundish is based here on a representation of the tundish geometry and materials, as illustrated in Fig. 2 [19]. Within this geometry, the melt behaviour is analysed according to its mass, momentum and energy conservation. The following assumptions and boundary conditions have been used, based on experimental observations and theoretical considerations:

- the melt flow is stationary and laminar,
- melt properties are constant within the temperature range considered in the submodel,
- at the exit point for the expanding cold gas flow the wall temperature is constant ($0\,^\circ C$),
- the wall temperature of the upper tundish is constant, and lower than the metal's solidus temperature.

The tundish model is used to calculate the heat loss by the melt between the upper free surface and the exit. Calculated results for various guide tube diameters and initial superheating melt temperatures (above liquidus) are illustrated in Fig. 3 for steel and copper materials. As the superheating of the melt increases, the temperature loss increases. In principle, the temperature losses are almost identical for steel and copper melts, although the copper melt is about 400 K colder than the steel melt.
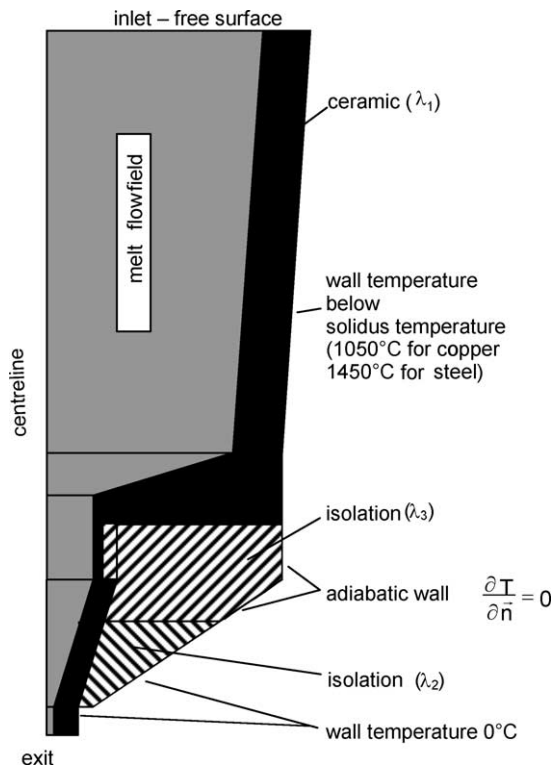
Fig. 2. Geometry and boundary conditions of the tundish model.
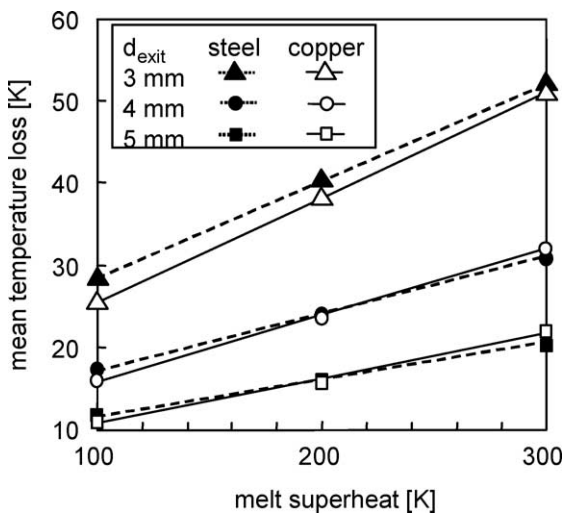

Fig. 4. Stages of droplet solidification model (low carbon steel).

Fig. 3. Mean temperature loss of the melt within the tundish for different melt superheats and guide tube diameters.

3. Spray simulation

To evaluate the thermal behaviour and properties of melt droplets in the flight phase within the spray, a multiphase flow simulation tool is used, based on the principle of an Eulerian/Lagrangian analysis of dispersed multiphase flows [5,20,21]. In this model, both the turbulent gas flow and the behaviour of the droplets are described simultaneously in a coupled way.
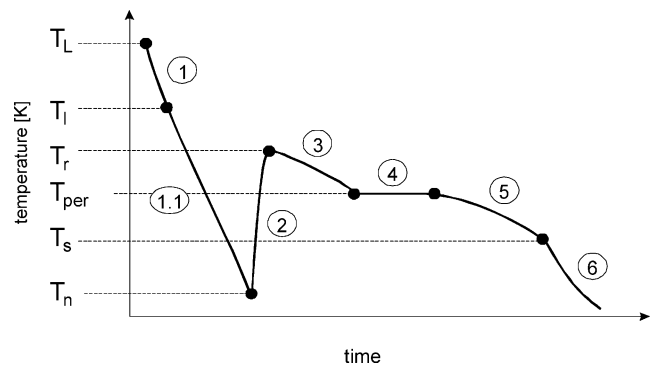
The gas phase is represented in a two-dimensional finite volume formulation with upwind discretization for convective terms. A staggered grid with up to ≈ 5000 grid cells is used. The standard $k–\varepsilon$ model is used for turbulence modeling. Source terms for momentum and thermal energy coupling between gas and particles are introduced using the PSI-approach [20].

The cooling and solidification of the melt droplets, as well as the consequent heating of the gas, are also considered. Cooling of the droplets takes the heat transfer by radiation and convection into account. The convective cooling process is described by means of the local Nusselt number

$$Nu = \frac{\alpha d_{\mathrm{p}}}{\lambda_{\mathrm{g}}} = 2 + 0.6Re^{1/2}Pr^{1/3}\left(1 + 3.4Tu^{0.843}\right) \qquad (1)$$

that contains the effect of local gas turbulence intensity Tu [5].

An alloy composition-dependent model of the solidification process within melt droplets of a spray is used, as has been described in [22]. Due to the high cooling rates of molten metal droplets in spray processes the process of delayed nucleation and therefore heavily undercooling of the droplets prior to nucleation and the onset of solidification has to be considered. The model derived in [22] describes the cooling and solidification process of a molten metal droplet within 6 stages as illustrated in Fig. 4 for the example of a low carbon steel droplet. After cooling in the liquid state (from the superheat temperature to the liquidus temperature), the droplet may be undercooled down to the nucleation temperature, where the first nuclei are built. In the second stage, after nucleation the drop temperature raises due to rapid release of latent heat. Further solidification after recalescence takes place with a decrease in droplet temperature until the peritectic temperature has been reached and the peritectic transformation at constant temperature occurs. Further segregated solidification takes place in the droplet after peritectic transformation. After the solidus temperature has been reached, the droplet is completely solidified and it further cools down in the solid state. Model assumptions and equations for the analysis of droplet cooling and solidification are listed in [22].

The spray model predicts the transient heat transfer and cooling behaviour of individual droplets along their flight
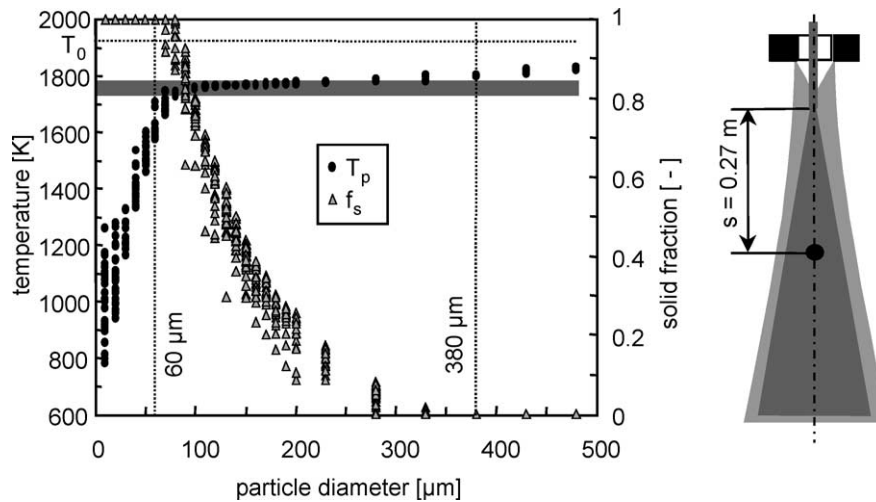
Fig. 5. Effects of particle diameter on calculated temperatures and solid fractions of individual particles at a point within the spray cone ($s = 0.27$ m, $r = 0$ m); standard parameters, the solidification interval of C30 steel is indicated in grey.

Table 1
Parameter sets

Parameter set	Material	p_g [MPa]	$\dot{M}_g$ [kg·s^{-1}]	M_L [kg·s^{-1}]	GMR [$-$]	ΔT_L [K]
Standard	C30	0.35	0.21	0.175	1.2	150
P1	C30	0.35	0.21	0.175	1.2	100
P2	C30	0.35	0.21	0.175	1.2	200
P3	C30	0.35	0.21	0.175	1.2	300

trajectories in the spray. The droplets are represented by parcels at increments of 10 μm. Consequently, the thermal state of the particles impinging on the deposit or substrate can be calculated. The results of a spray simulation are shown in Fig. 5. The calculated temperatures and solid fractions of individual particles of different sizes at a position along the centreline of the spray ($r = 0$ m) at a distance of $s = 0.27$ m below the point of atomization are illustrated (due to the geometrical arrangement of the atomizer, the atomization point is located at a distance of $z = 0.13$ m below the atomizer, therefore, the distance of $s = 0.27$ m corresponds to a distance from the atomizer, z, of 0.4 m). The process parameters used in this calculation are standard parameters for the spray-forming of C30 steel, as shown in Table 1.

From the data in Fig. 5, the following conclusions regarding the particle's thermal state with respect to the droplet diameter can be made:

$d_p < 60$ μm: All particles in this size range at the position under investigation are already fully solidified (solid fraction $f_s = 1$) and at temperatures below solidus temperature. As the particle size decreases, their temperature decreases as well, while the scattering of temperatures increases due to the particles' reduced inertia and mass, and the turbulent gas flow, which results in particle dispersion.

$60 < d_p < 380$ μm: In this droplet size range the particles are in the process of solidification ($0 < f_s < 1$). The thermal state of individual particles may vary as well: in the size range between 70 and 80 μm some fully solidified particles may be observed, while in the size range 270 to 330 μm some droplets that are still fully melted (fluid) may be found. Particles that are in the process of solidification have temperatures between the solidus and liquidus temperatures (this temperature region is indicated in the figure in grey). The solid fraction of particles decreases with increasing particle size.

380 μm $< d_p$:   All particles within this size range are still fully liquid at the position under consideration. Their temperature is above liquidus temperature, which means that they still contain some superheat. The amount of superheat increases with increasing particle size.

The spray model yields data related to the temperature and solid fraction of individual droplets within the spray. The droplets are divided into classes with properties (e.g., size) in certain ranges that collectively represent all particles within the spray. The mass contribution of the droplet classes on the total mass flux is taken into account. To derive the integral heat and mass fluxes from the spray to the deposit, the droplet data have to be averaged in a suitable manner.

Thermal averaging may be performed in two different ways, describing two extreme situations that occur in a molten metal spray [4]. The first averaging method (the enthalpy method) describes the thermal status of the particle mass in thermal equilibrium, here the thermal state of a certain particle mass is described after adiabatic equalization. This means the particle mass has a specific enthalpy which is directly related to its thermal state (temperature and solid fraction).

In a molten metal spray, situations may occur where the particle mass should already be fully solidified according to its average properties (when calculated by the enthalpy method), although it still contains some liquid. This may occur when the main spray consists of a large proportion of cold, solidified particles and only a small number of large, fluid, and hot melted particles. These liquid droplets still deliver a certain amount of liquid melt to the mushy layer on the deposit surface, which is not accounted for by the enthalpy method. However, if a separation averaging method is used, this deficit is avoided. Here, the amount of solidified mass or fluid melt mass remaining in the spray is calculated separately.

3.1. Averaging the particles' specific enthalpy (the enthalpy method, index h)

In this averaging approach, the specific heat content and the remaining latent heat content of each particle class i are summed to average the specific enthalpy $\overline{h_p}$ of the impinging spray. This approach yields the thermal equilibrium condition of the total droplet mass [23]:

$$\overline{h_p} = \frac{1}{\sum_i m_{p,i}} \sum_i \left\{ m_{p,i} \left[\left(c_{pl}(T_{p,i} - T_s) + \Delta h_f \right)(1 - f_{s,i}) \right.\right.$$
$$\left.\left. + c_{ps}\left((T_{p,i} - T_s) f_{s,i} + T_s \right) \right] \right\} \quad (2)$$

Based on the calculated average specific enthalpy $\overline{h_p}$ from Eq. (2), the mean spray solid fraction $f_{s,h}$ and the mean temperature T_h are calculated according to the solidification state of the droplet mass:

(a) If the droplet mass is fully solidified, the average specific enthalpy is lower than the specific enthalpy at solidus temperature T_s:

$$\overline{h_p} \leqslant c_{ps} T_s \implies f_{s,h} = 1, \quad T_h = \frac{\overline{h_p}}{c_{ps}} \quad (3)$$

(b) If the particle mass is in a state of phase change (solidification):

$$c_{ps} T_s < \overline{h_p} < c_{ps} T_s + c_{pl}(T_l - T_s) + \Delta h_f \implies$$
$$f_{s,h} = \frac{c_{ps} T_s + c_{pl}(T_h - T_s) + \Delta h_f - \overline{h_p}}{(c_{pl} - c_{ps})(T_h - T_s) + \Delta h_f},$$
$$T_h = \frac{\overline{h_p} + (1 - f_{s,h})[(c_{pl} - c_{ps})T_s - \Delta h_f]}{(1 - f_{s,h})c_{pl} + f_{s,h}c_{ps}} \quad (4)$$

The mean solid fraction can be calculated iteratively from the enthalpy method $f_{s,h}$ and the temperature of the enthalpy method T_h using the appropriate equilibrium phase diagrams. For pure metals, the mean temperature is equal to the constant solidification temperature ($T_h = T_s = T_l$).

(c) If the particle mass is still totally liquid, the mean specific enthalpy is greater than the specific enthalpy at liquidus temperature:

$$c_{ps} T_s + c_{pl}(T_l - T_s) + \Delta h_f \leqslant \overline{h_p} \implies$$
$$f_{s,h} = 0, \quad T_h = \frac{\overline{h_p} + (c_{pl} - c_{ps})T_s - \Delta h_f}{c_{pl}} \quad (5)$$

3.2. Averaging the solid fraction and temperature separately (the separation method, index m)

In the second averaging approach, the non-equilibrium situation in the spray process is recognised. The energy exchange within the total particle mass occurs only via the specific heat content and not via the remaining latent heat content of the particles:

$$f_{s,m} = \frac{1}{\sum_i m_{p,i}} \sum_i (m_{p,i} f_{s,i})$$
$$T_m = \frac{1}{(c_{ps} f_{s,m} + c_{pl}(1 - f_{s,m})) \sum_i m_{p,i}}$$
$$\times \sum_i \left(m_{p,i} T_{p,i} \left(c_{ps} f_{s,m} + c_{pl}(1 - f_{s,m}) \right) \right) \quad (6)$$

When considering a certain volume in which 50% of the mass consists of small, cold, and fully solidified particles, and the other 50% consists of a single large, fully fluid, and hot particle, then the separation method yields a mean solidification state as a solid fraction of $f_{s,m} = 0.5$ (regardless of individual temperatures or the latent heat contents of the single hot particle). For the enthalpy method, the mean properties are calculated in a coupled way. Here, the resulting mean temperature and the mean solid fraction depend on the difference between the small particles' temperature and the solidus temperature, and on the residual superheat remaining within the large particles.

Differences in the results obtained using the two averaging methods are shown in Fig. 6 for the averaged temperature and solid fraction of the spray along the centreline, as a function of the particle flight distance. The results of the enthalpy method represent the thermal equilibrium with respect to the particle mass. This occurs when bringing all particles from a specific location (point of impingement) together and leaving this mass under adiabatic conditions for an inner compensation process (heat conduction and solidification), obtaining the equilibrium values of T_h and $f_{s,h}$. This compensation process immediately occurs when the particle mass impinges on the deposit. In the mixing layer an equalization process will take place. Therefore, the enthalpy method properly describes the thermal state of the particle mass *in the mixing layer* after deposition. In contrast, the separation methods describes the instantaneous local thermal state (T_m and $f_{s,m}$) of the particle mass *in the spray*.

As can be seen in Fig. 6, for the whole particle flight distance the instantaneous mean particle temperatures and mean solidification fractions calculated by the separation model are lower than the values derived by the equilibrium state (enthalpy) method. With respect to the solidification process after the deposition this difference means that the
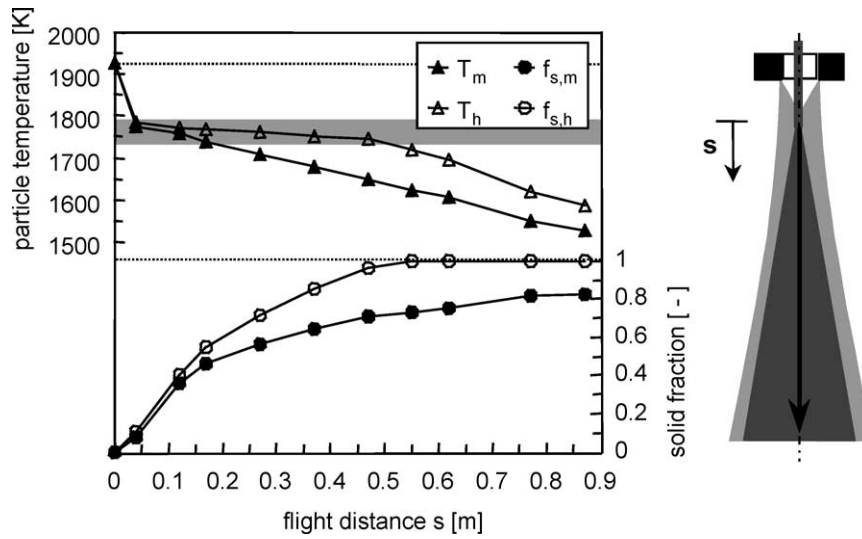
Fig. 6. Comparison of results of two averaging methods for calculating particle temperatures and solid fractions; mean averages for different particle diameters and flight distances (s), spray parameters = standard (Table 1).
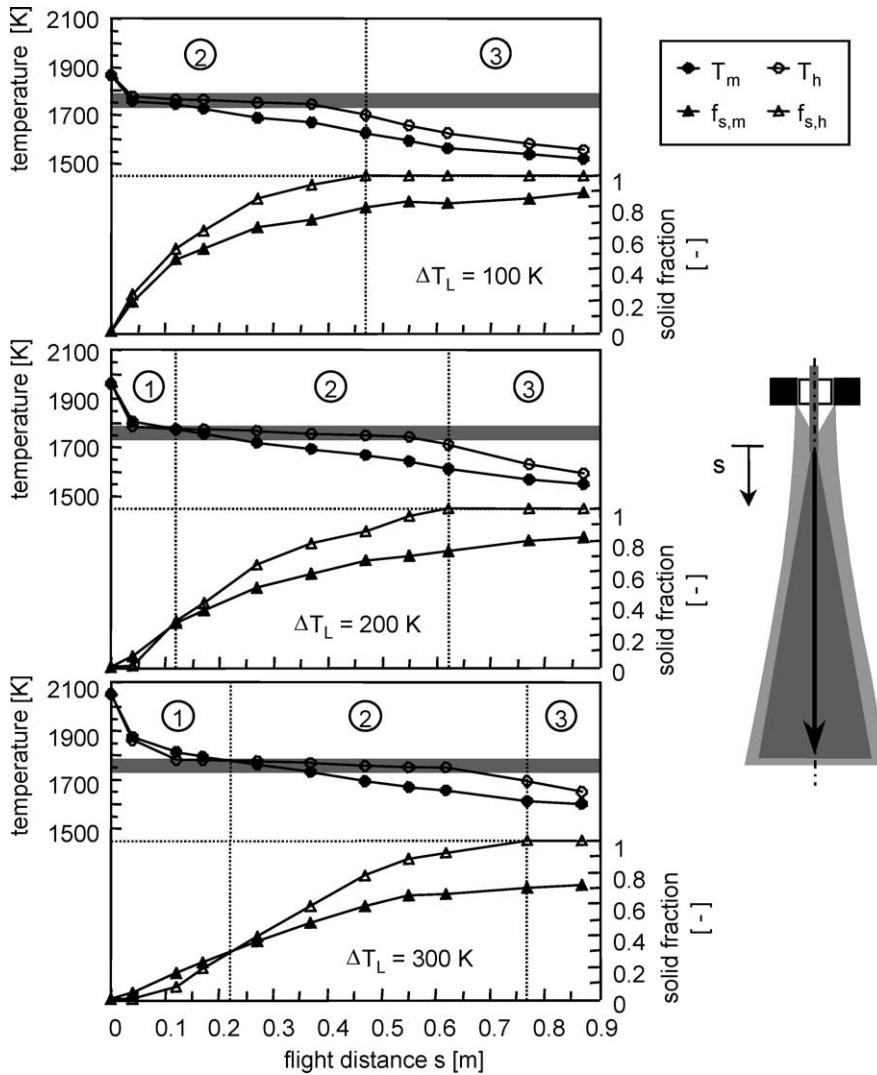

Fig. 7. Mean temperatures and solid fractions of the particle mass along the centreline of the spray's flight path for three different melt superheat values; comparison of different averaging methods for spray parameter sets P1 to P3 (Table 1).

overall particle mass is "undercooled" and may be reheated after the deposition (in the mixing layer) by the latent heat released during solidification.

To compare the results obtained by the two different averaging methods for the thermal properties of the particle mass along the spray centreline, the spray may be subdivided into three different zones:

Zone 1 Overheated spray ($T_m > T_h$; $f_{s,m} > f_{s,h}$).

In this zone, the values for temperature and solid fraction obtained by the separation method are greater than those obtained by the enthalpy method. For the overall particle mass this means that the calculated values for the solidification fractions tend to be too low, according to thermal equilibrium considerations. This implies, in turn, that if the spray particle mass within this zone is brought together during deposition, the remaining superheat from the larger, still liquid droplets will completely remelt the already solidified particle mass.

This overheated spray condition would result in an undesired increase of porosity and reduction of yield, as the spray particles during deposition may impinge on a more or less liquid pool, resulting in liquid droplet fragmentation and entrapment of gas bubbles.

Zone 2 Slightly undercooled spray ($T_m < T_h$; $f_{s,m} < f_{s,h}$).

In this zone, the results derived from the separation method are lower than the values obtained by the enthalpy method. The averaged particle temperature (with respect to the specific enthalpy) is in the range of the solidification interval ($T_s < T_h < T_l$). Therefore, in the state of thermal equilibrium after deposition the particle material in the mushy zone tends to have higher solid fractions. The remaining superheat in the bigger liquid drops is not sufficient to remelt parts of the already solidified particle material. However, the particle mass still contains enough enthalpy to ensure that even in the state of thermal equilibrium some melted parts will remain ($f_{s,h} < 1$).

Zone 3 Heavily undercooled spray ($T_h < T_s$; $f_{s,h} = 1$).

In this zone, the particle material in thermal equilibrium after deposition is completely solidified ($f_{s,h} = 1$). The equilibrium temperature is lower than the solidus temperature ($T_h < T_s$). In this zone the deposited material will be immediately solidified following deposition.

During spray formation, the spray may be compacted although the equilibrium state is already fully solidified. The remaining liquid in the spray (calculated by the separation method) still allows compaction in this zone of the spray. But the amount of cold porosity is increased in this zone.

The boundaries between these three zones can be shifted relative to the flight distance of the particles by adjusting the superheating of the melt in the crucible/tundish, as shown in Fig. 7. If the superheating of the melt is low ($\Delta T_l = 100$ K) the cooling of the particles occurs immediately after solidification. For this case zone 1 is not visible. The transition from zone 2 to zone 3 occurs at a flight distance of approximately $s = 0.47$ m. By increasing the melt superheating, this transition is shifted to greater flight distances ($s = 0.62$ m for $\Delta T_l = 200$ K and $s = 0.77$ m for $\Delta T_l = 300$ K). As superheating increases, zone 1 is established. The transition from zone 1 to zone 2 is located at a flight distance of $s = 0.12$ m ($\Delta T_l = 200$ K) and $s = 0.22$ m ($\Delta T_l = 300$ K). As the melt superheat increases, the zone transition is shifted towards increasing flight distances.

4. Thermal conditions inside the deposit

The deposit is built up through deposition of the impacting droplets/particles from the spray. The impacting particles deliver mass and heat to the deposit. The mass and heat flux contribution of the impacting particles as well as their particle size distribution strongly influences the cooling and processing of the material in the deposit [25–27]. Therefore, it is essential to derive the temporal enthalpy distribution inside the deposit during the compaction process and the following cooling process in order to describe the thermal history of a material element.

The model used in this investigation for the enthalpy distribution in the deposit is based on a model for calculating the temperature distribution in a growing deposit in combination with the underlying substrate [9,11]. The model is based on the numerical solution of the two-dimensional heat conduction equation on a non-orthogonal coordinate system fitting the transient deposit contour. The heat conservation equation includes a source term describing the release of latent heat during solidification. To investigate the influence of the substrate-to-atomizer distance on the thermal conditions in the deposit, calculations based on the standard parameter settings (Table 1) are performed. The deposit geometry under investigation is of Gaussian shape, resulting from normal impingement of the spray onto a circular disc. For the boundary condition at the deposit and substrate surface, the heat transfer due to convection and radiation is taken into account. The convective heat transfer coefficient has been correlated from measured heat transfer coefficient values in an atomizer gas jet flow [19].

By changing the distance between the atomizer and substrate, the thermal state of the particle mass is changed as well as the spray width (mass flux distribution). As this distance increases, the radial mass flux distribution becomes flatter and broader [24]. Thus, the dimensions of the deposit are changed, but its essential form remains the same. In the following discussion, the relative deposit height x/x_{max}
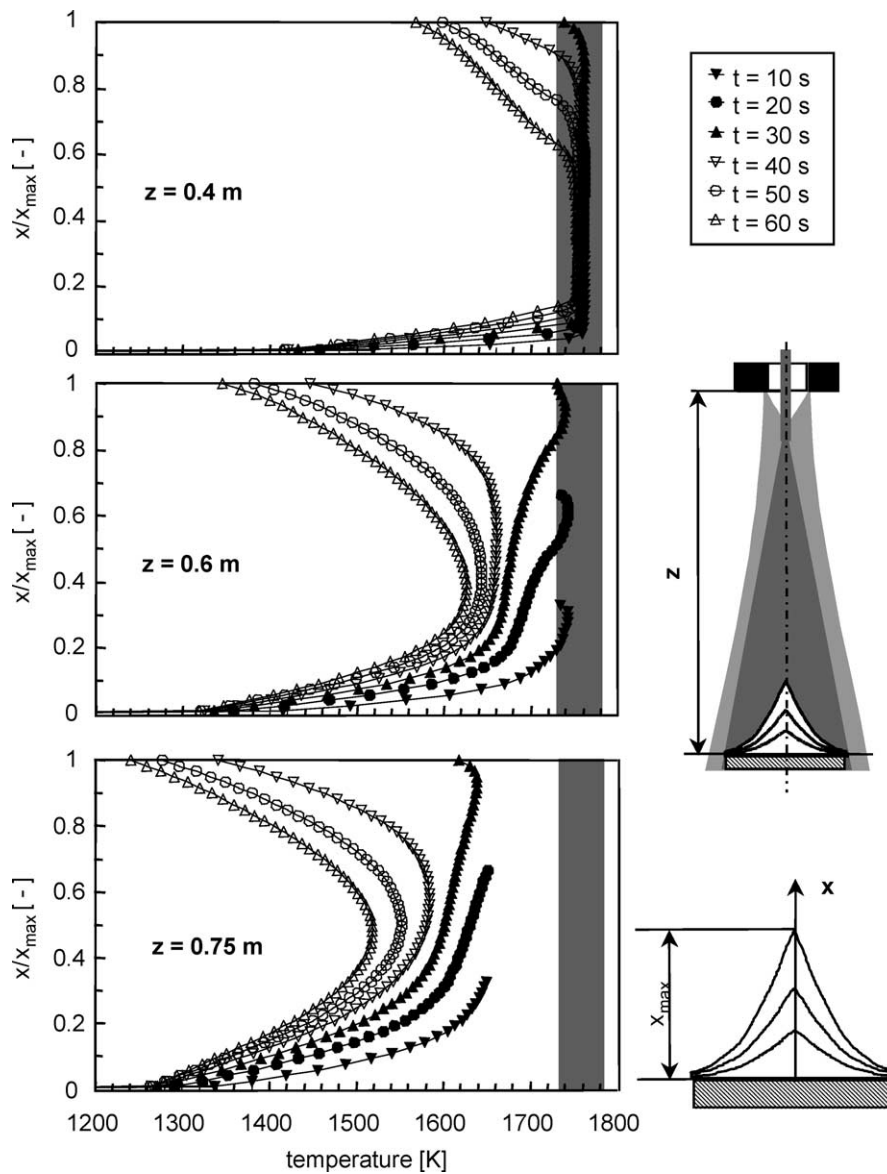
Fig. 8. Effects on the calculated temperature distribution along the centreline of the deposit of: the normalized distance x/x_{max} to the substrate surface, the time during the spray phase (10, 20 and 30 s, solid symbols) and the distance z to the atomizer. Spray parameters = standard (Table 1). The shape of the sprayed deposit in the sketch is shown at 10, 20 and 30 s. The spray phase is 30 s and the cooling phase is also 30 s.

(i.e., height in relation to the maximum deposit height) is used instead of the total deposit height x. For the standard spray condition in Table 1 the height of the deposit that has been actually sprayed was 0.132 m. Because the geometry of the deposit slightly changes with operational conditions, the relative height x/x_{max} is used for the discussion of the results.

Figs. 8 and 9 illustrate the temperature and solid fraction distribution along the centreline of the deposit for a spray time of up to 30 s and a subsequent cooling period of up to 30 s. It can be seen that by decreasing the substrate-to-nozzle distance the heat flux into the deposit is increased.

At a distance of $z = 0.4$ m, the material inside the deposit reaches temperatures that are within the solidification interval of the material $1733 < T < 1783$ K (grey shaded area) during the compaction period throughout the whole depth of the deposit. The temperature is below solidus only very close to the substrate ($x/x_{max} < 0.05$) (Fig. 8). Therefore, the solid fraction throughout the whole deposit depth ($0.05 < x/x_{max} < 1$) is smaller than 1 (Fig. 11) for a substrate located at this distance. The mixing layer, where material that is still melted is found, strongly increases during the growth of the deposit (compaction period).

During further cooling the material's temperature decreases, beginning from the deposit surface and the deposit/substrate interface. After 60 s the temperature of the material in the upper area of the deposit ($0.6 < x/x_{max} < 1$) is below solidus temperature, and the material is fully solidified. In the underlying region ($0.25 < x/x_{max} < 0.6$) the material is in the solidification state (semi solidified,
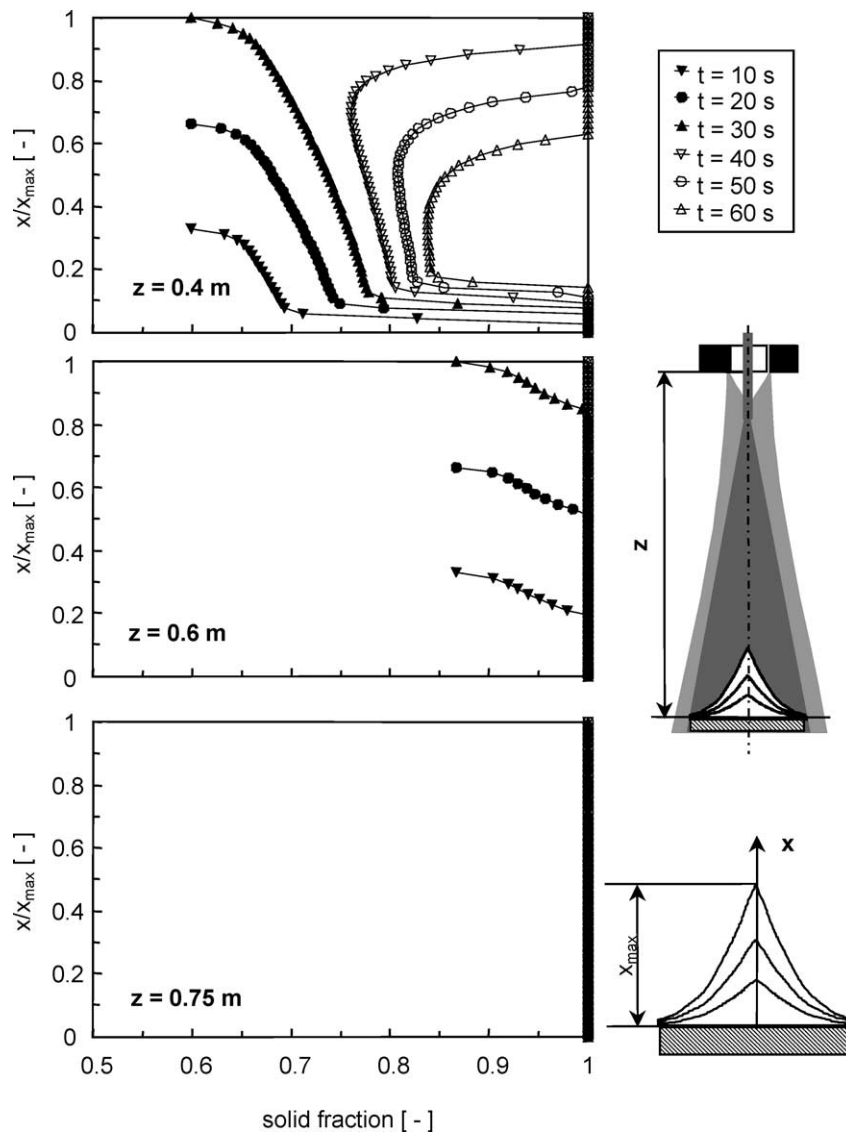
Fig. 9. Effects on the calculated solid fraction along the centreline of the deposit of: the normalized distance x/x_{max} to the substrate surface; the time during the spray phase (10, 20 and 30 s, solid symbols) and the distance z to the atomizer. Spray parameters = standard (Table 1). The shape of the sprayed deposit in the sketch is shown at 10, 20 and 30 s. The spray phase is 30 s and the cooling phase is also 30 s.

$0.84 < f_s < 1$) and the temperatures are within the solidification interval.

If the substrate-to-nozzle distance is increased to $z = 0.6$ m, the region where the temperature is in the solidification interval during the compaction time and the material is semi solidified is limited to a small layer at the top of the deposit:

$t = 10$ s: $0.21 < x/x_{max} < 0.33,\ 1733 \leqslant T \leqslant 1783$ K

$\qquad\qquad 0.87 \leqslant f_s < 1$

$t = 20$ s: $0.53 < x/x_{max} < 0.66,\ 1733 \leqslant T \leqslant 1783$ K

$\qquad\qquad 0.87 \leqslant f_s < 1$

$t = 30$ s: $0.85 < x/x_{max} < 1,\ 1733 \leqslant T \leqslant 1783$ K

$\qquad\qquad 0.87 \leqslant f_s < 1$

The thickness of the mixing layer at this distance ($z = 0.6$ m) only slightly increases. Almost 10 s after the end of the compaction time ($t = 40$ s) all of the deposited material is completely solidified. Temperatures are below solidus ($T < 1733$ K) and the solid fraction everywhere is 1. Inside the deposit a parabolic temperature profile has been established. At $z = 0.4$ and 0.6 m the substrate is located in the heavily undercooled zone of the spray.

By further increasing the nozzle-to-substrate distance to $z = 0.75$ m the particle material in the spray is so cold that the temperatures within the deposit do not stay in the solidification interval even during the compaction process. The material is completely solidified almost immediately after deposition ($f_s = 1$). Therefore, no mixing layer is established in this case, but spray compaction still occurs as the spray still contains some liquid melt.

5. Coupled model

The various spray-forming sub-models are coupled in order to analyse the behaviour of the melt material from melt superheating to room temperature via cooling and solidification. The time axis is shown in terms of the mass-averaged mean residence time of the particle mass in the spray. By combining these data with the calculated temporal cooling and solidification distributions of a fixed volume element inside the deposit, one obtains the mean thermal history of the material at a specified location in the deposit.

Transient thermal and solidification distributions are shown in Figs. 10 and 11, illustrating the three different modelling regions (melt flow in the tundish; particle cooling in the spray; growth and cooling of the deposit) at different time scales. The time t_0 is taken as the time where the melt element is at the top surface of the tundish. The temperature and solidification history of the melt element are described

for a time period of 100 s. The process conditions under consideration are listed in the standard parameter settings of Table 1 ($z = 0.6$ m, deposit centreline, $x/x_{max} = 0.5$). From the top of the tundish (upper melt surface) to the exit of the tundish in the atomization nozzle, the melt is cooled by ≈ 20 K (for an initial melt temperature of 1933 K). The solid fraction of the melt does not change as the melt stays fully liquid ($f_s = 0$). In total, the mean residence time of the melt in the tundish is 51.6 s for an exit diameter of $d_{exit} = 4$ mm and a surface height of $h = 0.25$ m for the melt in the tundish (determining the melt mass flow rate).

In the spray flow, the melt droplets are cooled mainly by convective heat transfer to the surrounding atomizer gas flow. Until impingement onto the substrate ($z = 0.6$ m is the distance from the atomizer, and $s = 0.47$ m is the distance from the atomisation point below the atomizer) the mean residence time of the particles in the spray is 0.011 s. In this time, the melt material is cooled down by 260 K
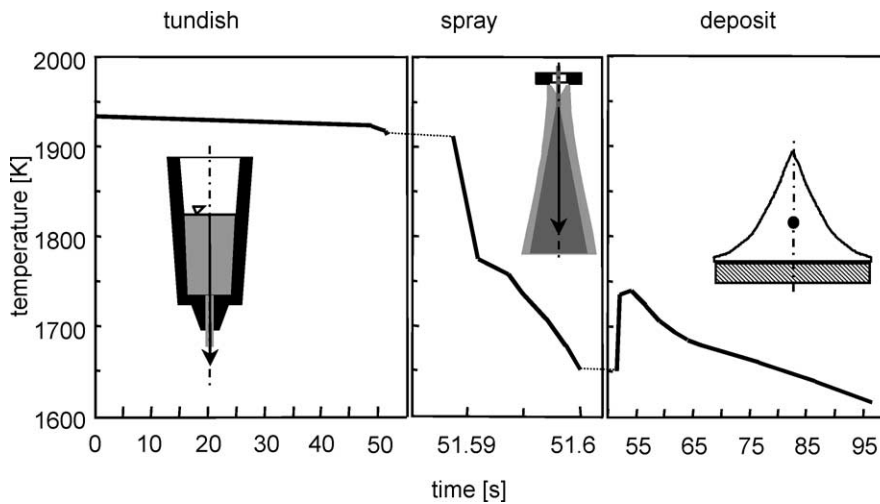

Fig. 10. Calculated mean material cooling curves in the three process steps. Spray parameters = standard (Table 1), spray distance $z = 0.6$ m, mid point of deposit at $x/x_{max} = 0.5$.
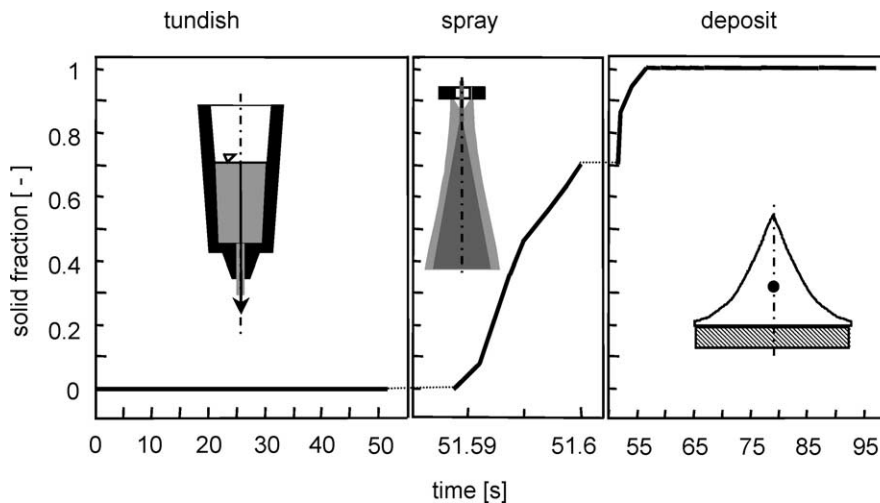

Fig. 11. Calculated mean material solid fraction in the three process steps. Spray parameters = standard (Table 1), spray distance $z = 0.6$ m, mid point of deposit at $x/x_{max} = 0.5$.

($T_m = 1650$ K) corresponding to a mean cooling velocity of 2.4×10^4 K·s^{-1}. Consequently, the solid fraction in the spray increases to $f_s = 0.71$.

Because of thermal diffusion and the release of latent heat inside the mixing layer of the deposit, the temperature of the material increases suddenly immediately after compaction when the material comes into equilibrium. For the discussed parameter settings the temperature increase is ≈ 90 K. After complete solidification of the volume element under investigation ($f_s = 1$), the temperature will then decrease again, at a cooling velocity of 2 to 3 K·s^{-1}.

If the standard process conditions are varied (parameters see Table 1), the thermal properties of the particle mass in the spray are responsible for consequent changes in transient cooling and solidification processes inside the deposit, as shown in Fig. 12. Here the temperature and solid fraction value of the melt element under observation is illustrated versus time on a linear scale. The dotted lines in the figures indicate the melt elements temperature and solid fraction values for the compacting particle mass immediately upon impact before consolidation in the deposit. For a distance of only $z = 0.4$ m, the compacting particle mass has a mean temperature of $T_m = 1707$ K and a mean solid fraction content of $f_s = 0.56$. Due to the high remaining liquid melt content, the volume element discussed here at the end of the time shown is not completely solidified ($f_s = 0.86$). Thus,

the temperature only decreases slightly, by ≈ 12 K within the solidification interval.

If the distance is increased to $z = 0.6$ m, the mean thermal conditions of the impacting mass are changed to $T_m = 1650$ K and $f_{s,m} = 0.71$. For a short time the temperature of the material reaches the solidification interval, and then decreases after finishing the solidification process.

At a distance of $z = 0.75$ m, the particle mass completely solidifies immediately after compaction. After a brief rise in temperature towards the solidification interval, the volume element cools down continuously. The material inside the deposit cools down faster in this case than it does for either of the other two nozzle-to-deposit distances considered.

As well as increasing mean temperatures, raising the melt superheat (parameter settings P1 to P3) increases the remaining melt content of the impacting particle mass (Fig. 13). Here also, the dotted lines in the figures indicate the melt elements temperature and solid fraction values for the compacting particle mass immediately upon impact. For a melt superheat of $\Delta T_L = 300$ K the remaining liquid melt content in the particles is sufficient to prevent the material inside the deposit from being completely solidified in the time shown here. The temperature remains in the solidification interval after reheating.

For a melt superheat of $\Delta T_L = 200$ K, the volume element discussed here is completely solidified after 66 s.
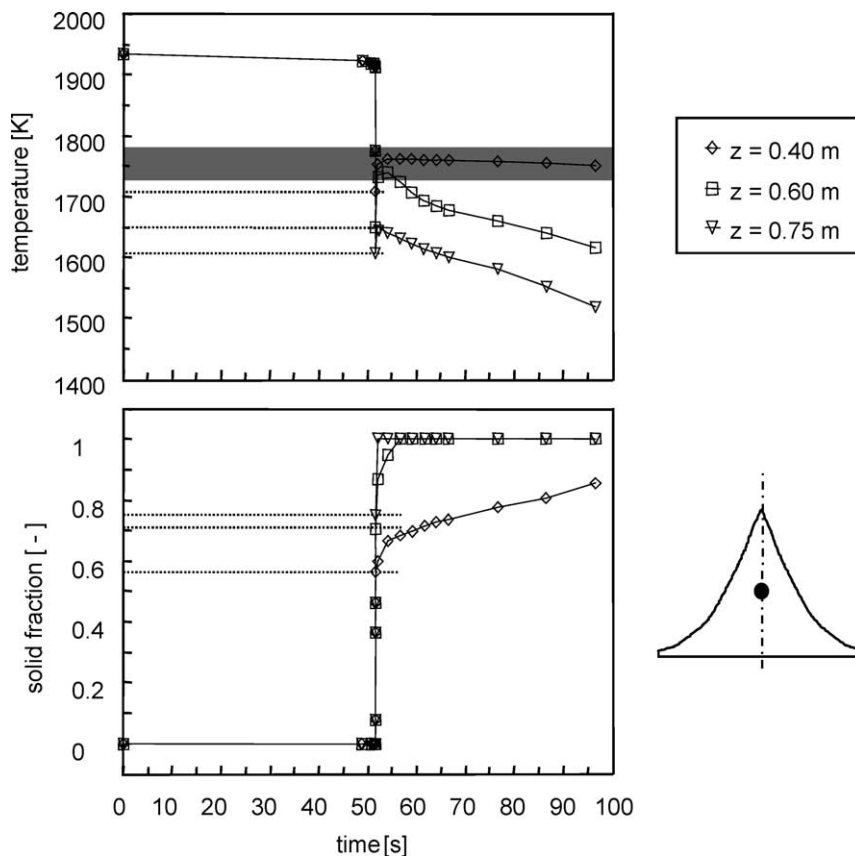

Fig. 12. Influence of the distance z between the atomizer and the substrate on the thermal history of a material element (spray parameters = standard parameters, Table 1).
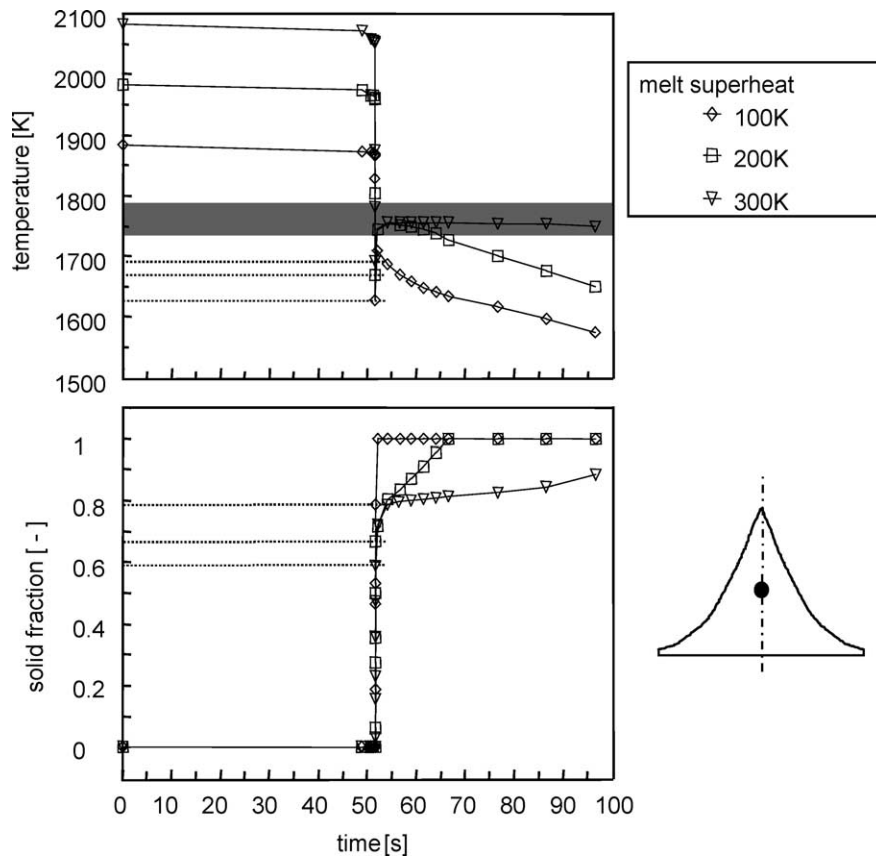
Fig. 13. Influence of the melt overheat on the thermal history of a material element (spray parameters = parameter sets P1 to P3, Table 1).

Before that, the temperature distribution peaks at $t = 54$ s (at $T = 1752$ K), following the increase that occurs during compaction, and then declines.

A melt superheat of just $\Delta T_L = 100$ K results in a sudden solidification of the material element after compaction. Too little latent heat is then released to raise the temperature of material above the solidus temperature. After a small increase in the temperature it drops immediately.

6. Summary

Sub-models describing different stages of the spray-forming process have been coupled to give an integrated thermal model of the process. The main aim of coupling simulations of spray-forming processes is to allow thermal analysis of the material's residence time and cooling/solidification rates, and of the build-up of the mixing layer during compaction of the impinging particles from the spray onto the deposit.

The spray analysis has shown that the particle size distribution in the spray can be classified into three different states (already solidified, partially solidified and still liquid). Thermal averaging of the impacting particle mass can be done using either the separation or the enthalpy method. A three-zone subdivision of the spray, depending on the process conditions is proposed. In the zone close to the

atomization area, the spray is still superheated, in the following zone the average spray condition is slightly undercooled. For higher nozzle distances the spray is highly undercooled.

Based on these submodels, the thermal behaviour of a melt material element of steel has been simulated during successive process steps (melt flow in the tundish; particle flight in the spray; compaction, growth of the deposit and cooling) with varying atomization nozzle-to-deposit distances and melt superheat values. The cooling rates of the material within all the stages of the spray-forming process are derived from these functions.

Acknowledgement

References

[1] A. Leatham, Spray forming: alloys, products, and markets, JOM 51 (4) (1999), web-edition: http://www.tms.org/pubs/journals/JOM/9904/ Leatham/Leatham-9904.html.

[2] E.J. Lavernia, Y. Wu, Spray Atomization and Deposition, Wiley, Chichester, England, 1996.

[3] P.S. Grant, Spray forming, Progr. Materials Sci. 39 (1995) 497–545.

[4] P.S. Grant, B. Cantor, L. Katgerman, Modelling of droplet dynamic and thermal histories during spray forming—I. Individual droplet behaviour, Acta Metall. Mater. 41 (11) (1993) 3097–3108; II. Effect of process parameters, Acta Metall. Mater. 41 (11) (1993) 3109–3118.

[5] D. Bergmann, U. Fritsching, K. Bauckhage, Simulation of molten metal droplet sprays, Comp. Fluid Dynamics J. 9 (2001) 203–211.

[6] J.H. Hattel, N. Pryds, J. Thorborg, P. Ottosen, A quasi-stationary numerical model of atomized metal droplets, Part I: Model formulation, J. Model. Simul. Mater. Sci. Eng. 7 (3) (1999) 413–430.

[7] P. Mathur, D. Apelian, A. Lawley, Analysis of the spray deposition process, Acta Metall. 37 (2) (1989) 429–443.

[8] N. Pryds, J.H. Hattel, J. Thorborg, A quasi-stationary numerical model of atomized metal droplets, II: Prediction and assessment, J. Model. Simul. Mater. Sci. Eng. 7 (1999) 431–446.

[9] O. Meyer, U. Fritsching, K. Bauckhage, Numerical investigation of alternative process conditions for influencing the thermal history of spray deposited billets, Internat. J. Thermal Sci. 42 (2003) 153–168.

[10] M. Gutierrez-Miravete, E.J. Lavernia, G.M. Trapaga, J. Szekely, A mathematical model of the liquid dynamic compaction process. Part 2: Formation of the deposit, Int. J. Rapid Solidification 4 (1988) 125–150.

[11] U. Fritsching, H. Zhang, K. Bauckhage, I—Numerical simulation of temperature distribution and solidification behaviour during spray forming, Steel Res. 65 (7) (1994) 273–278; II—Numerical results of temperature distribution and solidification behaviour during spray forming, Steel Res. 65 (8) (1994) 322–325.

[12] R.S. Minisandram, R.M. Forbes Jones, K.M. Kelkar, S.V. Patankar, W.T. Carter Jr., Prediction of thermal history of preforms produced by the clean metal spray forming process, Mater. Sci. Eng. A 326 (1) (2002) 184–193.

[13] R.D. Doherty, C. Cai, L.K. Warner-Kohler, Modeling and microstructural development in spray forming, Int. J. Powder Met. 33 (3) (1997) 50–60.

[14] S. Annavarapu, R.D. Doherty, Inhibited coarsening of solid–liquid microstructures in spray casting at high volume fractions of solid, Acta Metall. Mater. 43 (8) (1995) 3207–3230.

[15] W.D. Cai, E.J. Lavernia, Modeling of porosity during spray forming, Mater. Sci. Eng. A 226–228 (1997) 8–12.

[16] Z. Djuric, P. Newberry, P.S. Grant, Two dimensional simulation of liquid metal spray deposition onto a complex surface, Model. Simul. Mater. Sci. Eng. 7 (1999) 553–571.

[17] P. Mathur, S. Annavarapu, D. Apelian, A. Lawley, Spray casting: An integral model for process understanding and control, Mater. Sci. Eng. A 170 (1991).

[18] C.Y.A. Tsao, N.J. Grant, Modeling of the liquid dynamic compaction spray process, Int. J. Powder Met. 30 (3) (1994) 323–333.

[19] D. Bergmann, Modellierung des Sprühkompaktierprozesses für Kupfer- und Stahlwerkstoffe, Dissertation, Universität Bremen, 2000.

[20] C.T. Crowe, T.R. Troutt, J.N. Chung, Numerical models for two-phase turbulent flows, Ann. Rev. Fluid Mech. 28 (1996) 11–43.

[21] N.G. Muoio, C.T. Crowe, U. Fritsching, D. Bergmann, Modelling metal droplet sprays in spray forming, ASME FED 223 (1995) 111–115.

[22] D. Bergmann, U. Fritsching, K. Bauckhage, A mathematical model for cooling and rapid solidification of molten metal droplets, Int. J. Therm. Sci. 39 (2000) 53–62.

[23] C.G. Levi, R. Mehrabian, Heat flow during rapid solidification of undercooled metal droplets, Metal. Trans. A 13 (2) (1982) 221–234.

[24] V. Uhlenwinkel, M. Buchholz, K. Bauckhage, Particle mass flux in the spray cone of a free fall atomizer, in: TMS Annual Meeting, San Diego, California, USA, February 28–March 4, 1999.

[25] K. Bauckhage, Stand der Technik beim Sprühkompaktieren von Bolzen, HTM 52 (5) (1997) 319–331.

[26] P. Grant, A model for the factors controlling spray formed grain size, in: Sprühkompaktieren, Kolloquium des SFB 372, Band 3, Universität Bremen, 1998, pp. 83–92.

[27] C. Kramer, Die Kompaktierungsrate beim Sprühkompaktieren von Gaußförmigen Deposits, Dissertation, Universität Bremen, 1997.